ASEAN Engineering Journal

Full Paper

OPTIMAL LOAD FREQUENCY CONTROL OF INTERLINKED NONLINEAR POWER SYSTEM INTEGRATED WITH SMES-TCSC AND HVDC

Vivek Nath

Department of Electrical Engineering, University College of Engineering, RTU, 342010 Kota, Rajasthan, India

Article history
Received
02 October 2023
Received in revised form
01 January 2024
Accepted
01 April 2024
Published online
31 August 2024

*Corresponding author
nath.phd17@rtu.ac.in

Graphical abstract

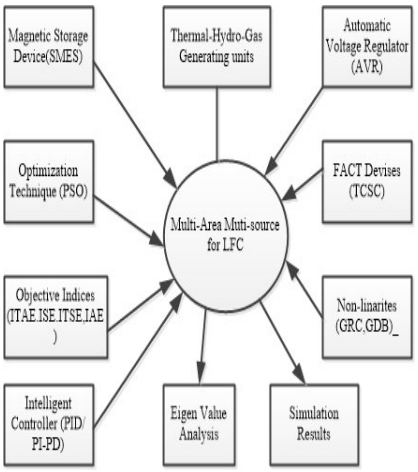

Abstract

In this article Multi-Area Multi-Source Interconnected Power System (MAMS-IPS) incorporated with an Automatic Voltage Regulator (AVR) in both the areas is considered for Load Frequency Control (LFC) study. Nonlinearity such as Governor Rate Constraints (GRC), Governor Dead Band (GDB), and Boiler are introduced with the thermal reheat generating unit. The effect of energy storage device (SMES) and fact device (TCSC) on the dynamic responses of IPS is also tested. PD-PID controller is suggested along with PID/PI-PD controller for minimizing the Automatic Control Error (ACE). The parameters of the proposed controller are optimized through a nature-inspired algorithm (PSO). PD-PID is superior then other suggested PID/PI-PD controllers. Objective functions ITAE, IAE, ISE, and ITSE are taken into consideration for finding the optimized values of the suggested controller as well as of TCSC and SMES devices. A step load of 10% is applied in both IPS areas. The rigidness of the suggested controller is verified by varying the loading condition of the IPS. A 10% increment in step load form is introduced for each area. The effect of renewable energy sources such as solar and a wind unit is also taken into consideration in this article. Varying step input is applied to this renewable unit to absorb its effect on the output responses of MAMS-IPS. The superiority of the PD-PID controller is verified by comparing its result with the recently published optimal controllers results described in the literature. SMES helps in improving the dynamic responses of the MAMS-IPS. Based on performance indices and Settling-time (ST) results of proposed controllers are compared with each other. For commenting on the stability of the introduced Power system (PS) eigenvalue analysis is also conducted. MATLAB version 2018 @ simulation software is used for simulation and for creating .m files

Keywords: Super Conducting Magnetic Energy Storage (SMES), Thyristor-Controlled Series Capacitor (TCSC), PD-PID Controller, GRC, GDB

1.0 INTRODUCTION

Modern electrical power system should be stable and reliable for supply uninterrupted power to user. Load Frequency Control (LFC) is a control mechanism utilized in power systems globally. Balance between power output and demand is to be maintained in a desirable limit. LFC work as a control nervous system for a interlinked power system. Complexity and size of the electrical grid is growing so it is very tidies task to maintain frequency at a desirable limit. Collaboration of renewable energy sources and conventional energy source is necessary in present scenario.

In this study, an Electric Power System (EPS) comprised of various generating units such as a Reheat-Turbine Thermal-unit, Hydro-unit, and Gas-unit as well as renewable energy sources such as wind and solar units are also integrated in each area For Load Frequency control (LFC) study. Because of their excellent effectiveness, Hydro and Thermal generating units are typically kept at base load, near to their maximum output. For boosting power system reliability and security gas power generation plays an important role as it responds very quickly to load variation. In an interlinked multi-source power system generating units and loads communicate with one another with the help of Tie-lines, which connects the areas. For the system

to operate efficiently, electricity generation must match total power demand plus energy losses. The purpose of LFC is to maintain the system frequency and Tie-line power exchanges between different control Zones at their acceptable values, for this LFC exchange and regulate power produced by different generating units in each area[1]. The objective of exploring Load Frequency Control derives is because it plays a vital role in modern power systems. As the energy scenery transforms with the combination of renewable resources like as wind and solar unit, as well as the growing of regionalized generation, the issues challenging LFC become more noticeable. Maintaining grid stability in the face of these changes is not only a technological necessity, but also a vital driver of economic growth and environmental sustainability. Frequent grid disturbances, if not cured suitably, can cause power outages, equipment damage, and economic losses. LFC research is motivated not just by technical attentions, but also by the crucial need to match power systems with environmental goals. Because power grids are becoming more complex, including the presence of micro grids and distributed energy resources, a more comprehensive and adaptive LFC structure is required.

In this study, AVR is incorporated in each area to maintain the output voltage of the generator at a desirable value. The excitation of field winding is changed to maintain the output voltage of the generator to an appropriate value. This is critical for keeping the electrical supply quality within tolerable levels to avoid overvoltage or under-voltage scenarios that could damage connected equipment or disturb power system steadiness. The secondary controller is required to minimize the Automatic Control Error (ACE), which is the sum of the product of the Biasing factor frequency deviation and Tie-Line power deviation. Classical controller such as PID, and PI is suggested For LFC is given in [2]. Integral double derivative controller (IDD) shows superiority over classical PID, PI controller its application for multi-area PS is illustrated in [3]. (1+PD)-PID cascade controllers are implemented for MAMS-IPS having Generating unit thermal, gas, and hydro for mitigation of frequency is given in [4]. Controller 2-DOF-PID parameters are optimized using an improved sine–cosine algorithm used for load frequency control of a three-area system having Nonlinearities as given in [5]. A tilt integral derivative controller proposed for two area interlinked PS is demonstrated in [6]. An intelligent controller such as a Fuzzy Logic controller (FLC) for two areas of interconnected power systems is demonstrated in [7, 8]. FLC for multi-area sources is illustrated in [9]. Performance analysis of ANFS for LFC is illustrated in [10]. NARMA-L2 controller application for two interlinked zones is given in [11]. For LFC, PID controller gains optimized by the Partial Swarm Optimization (PSO) Technique are given in [12]. As the governor action of the thermal and hydro generating unit is slow, even in the case of a small load deviation, it is very difficult to maintain the frequency deviation at its minimum point by adjusting the valve of the governor. As a result, the frequency and Tie line power deviations continue for a long period and are not feasible. To address this issue, Energy storage devices such as Super Conducting Magnetic Energy Storage (SMES) are introduced for LFC is given in [13, 14]. In this present work, SMES is introduced in both interlinked zones and its parameters are optimized by PSO to get an optimal result.

The attention of Power engineers' has been drawn toward Flexible AC Transmission System (FACTS) devices because of the rapid increase of power electronics components. It has the potential to increase the stability of the power system by controlling the power flow in an interacted power system. The thyristor-controlled phase shifter (TCPS) unit for Interlinked PS, integrating with energy storage systems known as redox flow battery (RFB) units are given in [15]. Load frequency control for MAMS-IPS using UPFC-SMES is given in [16]. communication time delays effect on the integrated LFC-AVR of a multi-area hybrid system with an IPFC-RFBs synchronized control scheme is demonstrated in [17]. The LFC united with SMES-TCPS and SSSC for an interlinked PS having a Hydro-Hydro unit is illustrated in [13, 18]. In this article, SMES-TCSC is incorporated with LFC-AVR to improve the output responses of IPS.

In this literature [19], MAMS-IPS is considered For LFC, But the effect of AVR, and HVDC is not included in its study and neither renewable energy sources are included. Eigenvalue analysis is also not conducted to verify system stability. The effect of HVDC-Link is not included in [20]. Nonlinearities (GDC, GRC), Energy storage device (ESD), Effect of Fact device, and Eigenvalue analysis are not considered in [21]. HVDC, ESD, and eigenvalue analysis are not considered in this[22]. In this literature renewable energy sources is also not demonstrated. In the presented work all these constraints are considered and the effect of their presence on LFC is studied. In this literature, LFC-AVR is considered but the effect of ESD, renewable energy units, and nonlinearity is not included in this study and also effect of wind and solar unit is also not investigated. Eigenvalue analysis is not explored in [23]. Fact Device and ESD are not concluded, neither eigenvalue analysis is taken into consideration in [24]. In this paper, all these points are included and their importance For LFC is justified. In this paper, a Proposed PD-PID controller optimized with PSO is implemented for a two-area multi-source interlinked (PS), and its effectiveness is verified by comparing with recently published findings such as DE-PSO-PID, HAEFA-PID, QEQS-PID, IWO-PID, PSO-PID optimal controller for the similar power system illustrated in [19, 20, 24-26].

Based on the prior explanation, the following are the main goals of the presented work.

1. Initially, for the LFC study, MAMA-IPS having generating units such as hydro, gas, and thermal is explored having Nonlinearities such as Boiler, GDB, and GRC.
2. The model is further modified by Incorporating Wind and Solar units in each area and a step load is applied as input to see it effect.
3. AVR is incorporated in both areas for maintaining generator excitation.
4. PSO-based PD-PID controller is suggested for Reducing the ACE Error following with PI-PD and PID proposed controllers
5. Energy storage Device (SMES) is also included in both zones to improve the PS output response deviation. Fact Device (TCSC) is incorporated with Tie-Line and its parameters are tuned By PSO optimized technique. HVDC link is interlinked with AC-Link in this presented work and its effect is investigated.
6. The robustness of the proposed controller is tested at different load variations. For verifying the stability of the proposed models, eigenvalue analysis is also conducted for all different cases.

7. Result of the proposed controller are compared with the result of controllers presented in recently published literature

2.0 SYSTEM DESCRIPTION

In this article, the proposed model consists of diverse sources such as thermal, hydro, and gas units. Both the area is interlinked using Tie-Line. A load perturbation in the form of a step is applied to each zone. Nonlinearity such as governor dead band (GDB), governor rate constraints (GRC), and boiler are incorporated with the thermal unit. For reducing the ACE error optimized PID/PI-PD/PD-PID controllers are proposed for this study. The parameters of the proposed controller are optimized using the PSO algorithm. For analyzing the effect of renewable energy sources such as wind and solar units are also integrated with the other generating units. Varying step input is given to wind and solar generating units. SMES energy storage unit is also included in this suggested model to mitigate the deviation in the output response. For analyzing the voltage output of the generator, the AVR control loop is also integrated in each area. Every transfer function is accomplished with a constant given in a second. HVDC-Link incorporated with AC-link is also included in the proposed MAMS-IPS. The transfer function model of MAMS-IPS incorporating with nonlinearities and renewable energy sources is illustrated in Figure 1.
The Third Order (TF) equation for Thermal Reheat Turbine is given below in Equation 1, Governor time constant is given by T_{gre}, Reheat Turbine Time constant is shown as T_{re} and T_t.

Gain of the reheat thermal unit is given by K_{re}

$$G_T(\mathrm{s}) = \frac{(1+s\,\mathrm{T}_{re}\mathrm{K}_{re})}{(1+s\,\mathrm{T}_{gre})(1+s\,\mathrm{T}_{re})(1+s\,\mathrm{T}_{tr})} \quad (1)$$

The Third Order (TF) Equation for Hydro Turbine is given below by Equation 2, T_{gh} T_{rh} and T_w is the Time-constant of the hydro unit

$$G_H(\mathrm{s}) = \frac{(1+\mathrm{sT}_{rs})(1-\mathrm{sT}_w)}{(1+s\,\mathrm{T}_h)(1+s\,\mathrm{T}_{rh})(1+0.5\,\mathrm{T}_{ws})} \quad (2)$$

The Fourth-order equation for Gas Turbine in the form of (TF) is given below in Equation 3, B and C are gain of the gas turbine. The lead-lag Time constant of the Governor is given by X and Y. T_{cr} Represented the combustion reaction Time constant and the Fuel time constant is given by T_f. Compressor Discharge volume Time-constant in (sec) is denoted by T_{CD}.

$$G_G(\mathrm{s}) = \frac{(1+\mathrm{xs})(1-T_{CR}\,\mathrm{s})}{(1+ys)(\mathrm{c}+\mathrm{bs})(1+\mathrm{T}_F\mathrm{s})(1+\mathrm{T}_{CD}\mathrm{s})} \quad (3)$$

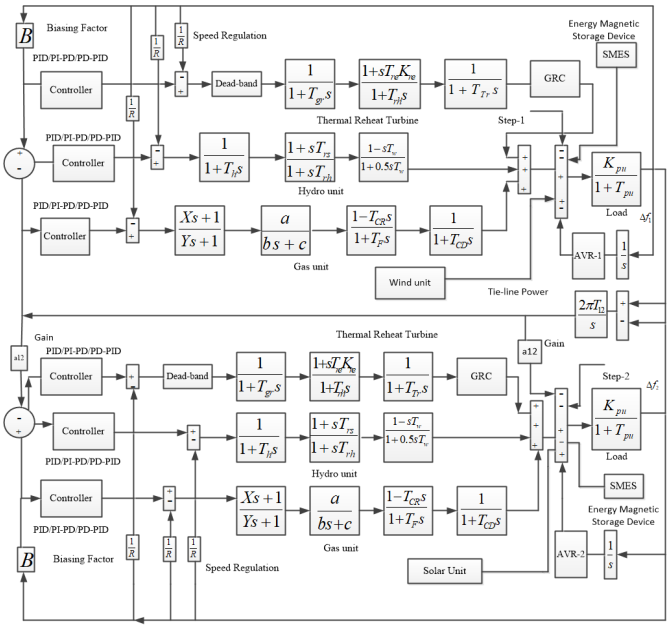

Figure 1 Interlinked Multi-area Power System with Renewable Energy Source

2.1 Modeling of AVR

Synchronous generator voltage at a specific value is maintained by the AVR control loop. Figure 2 gives a detailed AVR model with cross-coupling coefficients. Output voltage V is compared with reference voltage V_{ref} to measure the error voltage ΔV. The error voltage is amplified and directed towards the exciter to modify the generator field excitation, Because of this, any variation in terminal voltage is punctually corrected, resulting in system stability. In AVR, each subsystem is modeled as follows. The first order Transfer Function (TF) equation for the Amplifier is given below in Equation 4, where K_A is amplifier Gain and T_A is the time constant of the Amplifier.

$$G_A(\mathrm{s}) = \frac{K_A}{1+sT_A} \quad (4)$$

The First Order (TF) equation for Exciter is given below in Equation 5, where K_E define the gain and T_E is the time constant of the Exciter

$$G_E(\mathrm{s}) = \frac{K_E}{1+sT_E} \quad (5)$$

The First Order (TF) equation for the Sensor is provided below by Equation 6, K_s which defines the gain and T_s is the time constant of the Exciter

$$G_s(\mathrm{s}) = \frac{K_s}{1+sT_s} \quad (6)$$

The First Order (TF) equation for the Generator is provided below in Equation 7, where K_G define the gain and T_G is the time constant

$$G_G(s) = \frac{K_G}{1+sT_G} \tag{7}$$

The voltage Error signal is given by Equation 8

$$\Delta V = V - V_{ref} \tag{8}$$

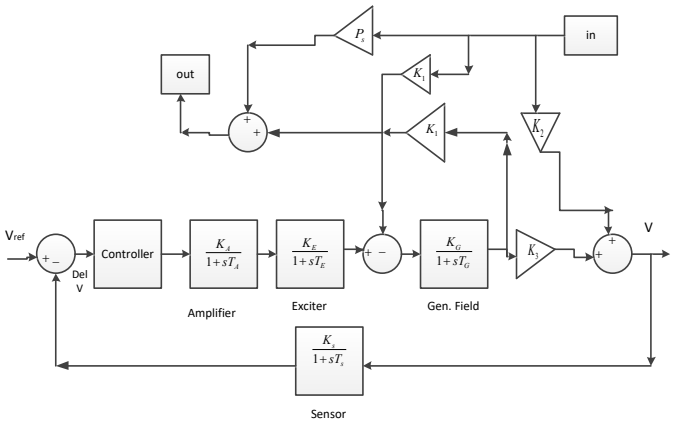

Figure 2 Automatic Voltage Regulator

2.2. Nonlinearities Integrated With MAMS-IPS

In MAMS-IPS mainly three nonlinearities are included first is GRC, second is GDB, and third is boiler. By imposing Governor Rate Constraint a stable and responsive control system can be created. It involves understanding the physical constraints of system components, modelling their behaviour, and developing control approaches that respect these constraints while achieving the proposed control objectives. A governor rate constraint helps the governor to change its output slowly and in a given band as the load varies [27, 28]. In this presented work upper limit of the band is taken as (0.5×10^{-2}) and the lower band is taken as (-0.5×10^{-2}). The block diagram of the GRC presented For LFC is demonstrated in Figure 3. A governor dead band is a range near a reference point in which the governor does not take any control action. It is a range of control signal values in which the control system is inactive, which does not allow the controller to take any action. Dead bands are frequently employed to avoid slight and negligible changes in the controlled variable from activating continual control actions, which could contribute to early wear on actuators and control mechanisms [29, 30]. In this suggested Model GDB Upper Limit is (0.8) and the Lower Limit is (-0.06) All values are in per-unit. The block diagram for GDB is illustrated in Figure 4. Boilers are essential in converting heat energy into electrical energy in a thermal power plant. Thermal power plants generate electricity by changing heat from the burning of fossil fuels such as coal, oil, natural gas, or nuclear reactors into steam. This steam is then consumed to power turbines, which are connected to generators to produce energy. The most common form of boiler used in thermal power plants is known as a steam boiler. The Block Diagram employed for the thermal generating unit is given in Figure 5.

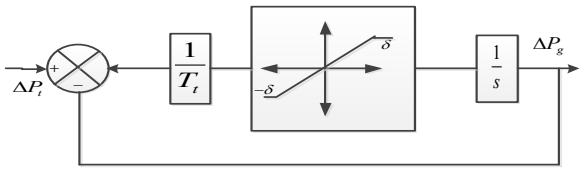

Figure 3 Block Diagram of Governor Rate constraints (GRC)

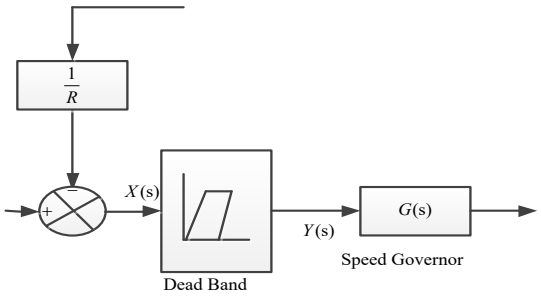

Figure 4 Block Diagram of Governor Dead Band (GDB)

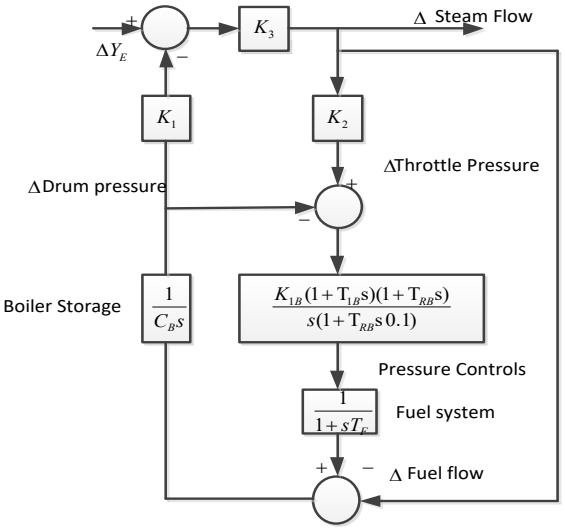

Figure 5 Block Diagram of boiler For Reheat Thermal Unit

2.3. High Voltage Direct Current

A single-line Structure of a two-area power system (PS) is illustrated in Figure 6 for governing DC-Line power flow, The Inverter and rectifier are integrated with DC-Line work as switching devices for HVDC system. Power Flow through AC and DC Tie-Line is given as $\Delta P_{tie1,2ac}$ and $\Delta P_{tie1,2dc}$ respectively.DC-Line First order transfer function is given by Equation 9.

$$\Delta P_{tie,dc} = \frac{K_{DC}}{1+sT_{DC}} \tag{9}$$

K_{DC} Indicates HVDC model Gain, T_{DC} Time constant of HVDC line.

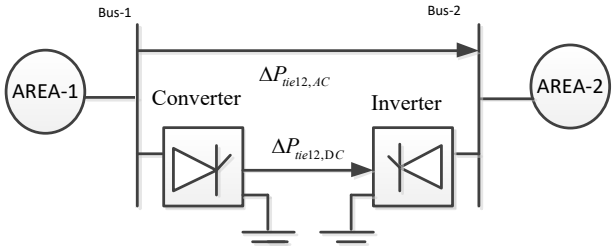

Figure 6 Block Diagram OF HVDC System for Two Area Power System

The exact HVDC Link Transfer Function (TF) is given in Figure 7 which is implemented in MAMS-IPS.

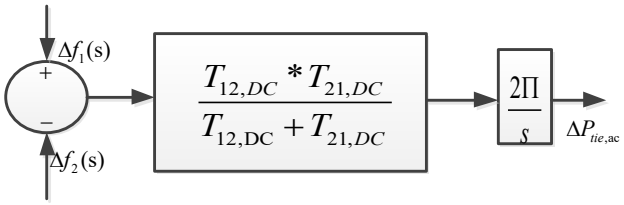

Figure 7 Transfer Function model OF HVDC

T_{12} and T_{21} are equivalent synchronizing factors of the HVDC Link. Detailed modeling of the HVDC Transfer Function (TF) For LFC is demonstrated in this reference.

2.4. Thyristor Controlled Series Capacitor

A Thyristor Controlled Series Capacitor (TCSC) is a power system device that regulates the capacitive reactance (X_c) of a transmission line to adjust its impedance. In electrical power systems, TCSCs are used to improve the stability, and performance of PS. They are generally engaged in power systems to control the power flow, voltage stability, and oscillation damping. A TCSC is made up of a capacitor bank that is associated in series with the transmission line, and its capacitive reactance can be changed using thyristor-controlled switching devices. Detailed modeling of TCSC for LFC is discussed in [19, 25, 31].

The flow of current is modeled and expressed by Equation 10, the flow of current is between area-1 and area-2.

$$I_{12} = \frac{|v_1|\angle(\delta_1) - |v_2|\angle(\delta_2)}{j(x_{12} - x_{TCSC})} \quad (10)$$

X_{12} is Tie-Line reactance

X_{TCSC} is TCSC reactance

$$\Delta P_{tie12} = \frac{J_{12}}{(1-K_{pc})^2}\Delta K_{pc} + \frac{T_{12}}{(1-K_{pc})}(\Delta\delta_1 - \Delta\delta_2) \quad (11)$$

$$\Delta\delta_1 = 2\pi\int \Delta f_1.dt \quad (12)$$

$$\Delta\delta_2 = 2\pi\int \Delta f_2.dt \quad (13)$$

Taking the Laplace transform of the above Equation (11)

$$\Delta P_{tie12}(s) = \frac{J_{12}}{(1-K_{pc})^2}\Delta K_{pc}(s) + \frac{2\pi T_{12}}{s.(1-K_{pc})}(\Delta f_1(s) - \Delta f_2(s)) \quad (14)$$

By using Equation 14 a transfer function model is structured which is shown below in Figure 8.

The Linearized model of TCSC is modeled and expressed by Equation 15

$$\Delta k_{PC}(s) = \frac{K_{TCSC}}{1 + sT_{TCSC}}\Delta E(s) \quad (15)$$

K_{TCSC} = Gain of TCSC constant

T_{TCSC} = The time constant of TCSC

TCSC controller is equipped close to area-1 in the Transmission-Line, Δf_1 which is taken as an error. $\Delta E(s)$ is an error signal, $\Delta K_{pc}(s)$ output signal

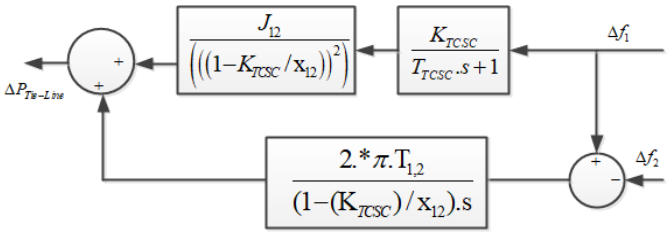

Figure 8 Block diagram of TCSC implemented with Tie-Line Power of IPS

2.5. Super Conducting Magnetic Energy Storage

TheSuper Conducting Magnetic Energy Storage (SMES) plays a dynamic function to assure improved system performance and provide a substitute choice to reduce oscillations effectively in the power system. SMES units are capable of handling both active and reactive powers at the same time to enhance the active and transient responses of generators in interlinked power zones. These devices have a feature to charge themselves at the time of off-peak hours and the stored energy can be consumed at the time of peak hours. It delivers storage capacity in addition to the kinetic energy (K.E) of the generator rotor, allowing it to share abrupt dissimilarities in power demand.

It is made up of a superconducting magnetic coil that stores electric power. SMES installed in each area to mitigate the frequency response (Δf) variation. K_{SMES} Define as the stabilizing gain and K_1, K_2 K_3 and K_4 are Time-constant for the lead-lag compensator used by SMES [13, 31, 32]. Values of this are tuned by using the suggested algorithm (PSO). SMES is used as a frequency preservative [14]. SMES lead lad compensator internal structure is shown in the Figure 9.

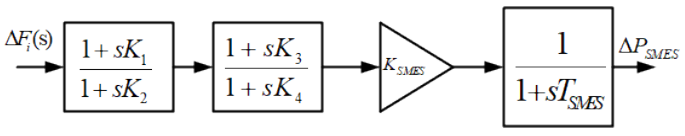

Figure 9 Lead Lag compensator structure OF SMES for LFC study [13]

2.6. Renewable Energy Sources

The PV panel includes a group of array of PV modules, each unit is a collection of cells that affect the output energy, and all units are impacted by the solar radiation of the sunshine. The First-order model of the PV equation has been shown in Equation 16. The simulation model was used to create the wind diversion system. The First-order model of a wind turbine is given by Equation 17. A step Disturbance of $\pm$ 1% is given to each solar and wind unit. Detailed analysis of wind and solar units for LFC is given in [33-35].

$$G_{pv}(\mathrm{s}) = \frac{K_{pv}}{1+sT_{pv}} \tag{16}$$

$$G_{TWG}(\mathrm{s}) = \frac{K_{WT}}{1+s.T_{WT}} \tag{17}$$

3.0 SUGGESTED METHODOLOGY

The PID controller is regularly employed Because of its simplicity, effectiveness, and adaptability towards a wide range of control systems. The proportional term generates an output that is directly proportional to the current error. This error is shown as a difference between the planned set-point and the present process value. The more the error, the greater the control effort required. The integral term accounts for the gathering of previous mistakes over time. It aids in the removal of steady-state errors (SSE) caused by constant instabilities. The integral term integrates the error over time and results in a corrective action proportionate to the error's integral. The derivative term calculates future errors by taking the rate of change of error into account. With the help of the derivative component, overshoot is reduced, and restrained the system's response to rapid changes. The derivative term is relative to the rate of change of the mistake. In this research article, a PD-PID controller is suggested along with the PI-PD and PID controller. The PD-PID controller is more efficient as compared to the PI-PD and Conventional PID controller. The gains of this controller are optimized using a fast-acting algorithm known as PSO. To provide the finest transient and steady-state performance while removing system errors, improved variants of PID such as PD-PID have been implemented for IPS. The theory of PD-PID controller is taken from this literature [36, 37].

For evaluating the fitness of the presented PSO algorithm, performance indices such as ITAE, ITSE, IAE, and ISE are taken into consideration. The objective Functions taken into consideration for optimizing the controller parameters are given in Equations 20 to Equation 23. The automatic control error (ACE) is given as input to the proposed controller. The Automatic Control Error (ACE) is given by Equation 18 and Equation 19. The PD-PID optimization Technique is demonstrated in Figure 10.

$$ACE_1 = \Delta P_{tie1,2} + B_1\Delta f_1 \tag{18}$$

$$ACE_2 = \Delta P_{tie1,2} + B_2\Delta f_2 \tag{19}$$

$$J_{ISE} = \int_0^T (\Delta f_1^2 + \Delta f_2^2 + \Delta v_{t1}^2 + \Delta v_{t2}^2 + \Delta P_{tie12}^2).dt \tag{20}$$

$$J_{IAE} = \int_0^T (|\Delta f_1| + |\Delta f_2| + |\Delta v_{t1}| + |\Delta v_{t2}| + |\Delta P_{tie12}|).\mathrm{dt} \tag{21}$$

$$J_{ITAE} = \int_0^T \mathrm{t}.(|\Delta f_1| + |\Delta f_2| + |\Delta v_{t1}| + |\Delta v_{t2}| + |\Delta P_{tie12}|).\mathrm{dt} \tag{22}$$

$$J_{ITSE} = \int_0^T \mathrm{t}.(\Delta f_1^2 + \Delta f_2^2 + \Delta v_{t1}^2 + \Delta v_{t2}^2 + \Delta P_{tie12}^2).\mathrm{dt} \tag{23}$$

The range of optimized Parameters is defined by us in this presented work the range for the proposed controller is considered between (-2 to 2)

$$K_{\mathrm{p1min}} \le K_{p1} \le K_{\mathrm{p1max}}$$

$$K_{\mathrm{d1min}} \le K_{d1} \le K_{\mathrm{d1max}}$$

$$K_{\mathrm{p2min}} \le K_{p2} \le K_{\mathrm{p2max}}$$

$$K_{\mathrm{Imin}} \le K_{I} \le K_{\mathrm{Imax}}$$

$$K_{\mathrm{d2min}} \le K_{d2} \le K_{\mathrm{d2max}}$$

Similarly, optimized parameters are found by implementing the PSO algorithm.

$$K_{1\min} \le K_1 \le K_{1\max}$$

$$K_{2\min} \le K_2 \le K_{2\max}$$

$$K_{3\min} \le K_3 \le K_{3\max}$$

$$K_{4\min} \le K_4 \le K_{4\max}$$

Similarly, TCSC's best parameters are found by implementing the PSO algorithm.

$$K\_smes_{\min} \le K\_smes \le K\_smes_{\max}$$

$$\mathrm{T}\_smes_{\min} \le T\_smes \le T\_smes_{\max}$$

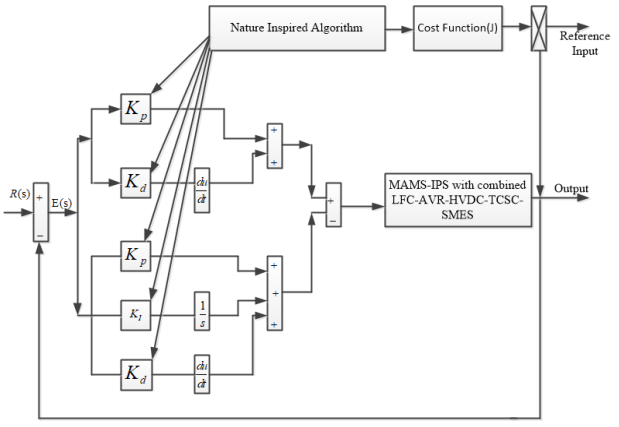

Figure 10 Block Diagram of Proposed Optimization Technique for PD-PID

4.0 PSO OPTIMIZATION TECHNIQUE

Particle Swarm Optimization (PSO) is a nature-inspired optimization technique in which the social behavior of birds

and fish is taken into consideration. Every particle lives in a group and communicates with each other to find the best solution. PSO was first introduced by Dr. Eberhart and Dr. Kennedy in 1995[38-40]. The algorithm mimics how birds in a group or fish in a Flock change their actions to find better nursing spots based on their neighbors' performance. The detail of the PSO algorithm for LFC to optimize the Gain is described in [38].

4.1 Steps showing how the PSO algorithm works

- Initialization

In the search space population of a particle is assigned a random position.Every particle is assigned a random velocity. The personal best positions of each particle are set as their initial positions. The initial position of each particle fitness is accessed by using an objective Function

- Setting a Global best

The highest fitness value in the population is determined by the particle. This particle's position is set as the best in the world.

- Update the iteration

Based on the following equation velocity and position of each particle are updated. The particle updated position is defined by Equation 24 and the velocity updated value is illustrated by Equation 25.

$$x_i(t+1) = x_i(t) + v_i(t+1) \quad (24)$$

$$v_i(t+1) = wv_i(t) + c_1(P_i(t) - x_i(t)) + c_2(g(t) - x_i(t)) \quad (25)$$

$$v_{ij}(t+1) = wv_{ij}(t) + r_1 c_1(P_{ij}(t) - x_{ij}(t)) + r_2 c_2(g_{ij}(t) - x_{ij}(t)) \quad (26)$$

$$x_{ij}(t+1) = x_{ij}(t) + v_{ij}(t+1) \quad (27)$$

$$W = \frac{Max_{iteration} - I_{iteration}}{Max_{iteration}} \quad (28)$$

Where v_i and x_i are the Velocity and position of a particle at the i^{th} position, j is the dimension. c_1 and c_2 are the acceleration coefficient. r_1 and r_2 are the casual number their range lies between 0 and 1. w Represents the inertia weight factor, illustrated in Equation 28. $Max_{iteration}$ Shows the maximum number of iterations and $I_{iteration}$ represents the current value of iterations. $c_1(P_i(t) - x_i(t))$ Represents cognitive elements, $c_2(g(t) - x_i(t))$ represents social elements. Equation 25 and Equation 26 show an increment in the position and velocity of a particle in two dimensions. Examining mechanism of the PSO technique is shown in Figure 11.

- Update Personal Best and Global Best

Its personal best fitness is compared with each particle's fitness; update the personal best position and fitness if the new fitness is better than the previous. The fitness of each particle is compared with the fitness of the present global best; update the global best position and fitness if any particle's fitness is better.

- Termination

When the fitness improvement becomes negligible or a set number of iterations is reached the algorithm is terminated

- Output

The global best position of the particle represents the optimal solution to the problem.

Parameters defined by us for optimizing PS0-PD-PID Controller $c_1 = 1.5, c_2 = 1, w_{max} = 0.3, w_{min} = 0.1$ the range for Controller is taken Between (-2 to 2) and For SMES the range is taken Between (0 to 2) similarly For TCSC the range is taken Between (0 to 1). $Max_{iteration} = 100$, $N_{pop} = 100$. Best solution value for different cases obtained while optimizing PD-PID by PSO optimized technique. **LFC-AVR-SMES** = Case-01, $Best\_cost = 5.768791$,LFC-AVR-SMES-HVDC=Case-02 its $Best\_cost = 4.70081$ LFC-AVR-SMES-TCSC = Case-03 $Best\_cost = 3.90771$, LFC-AVR-SMES-HVDC-TCSC=Case-04 $Best\_cost = 3.01507$.

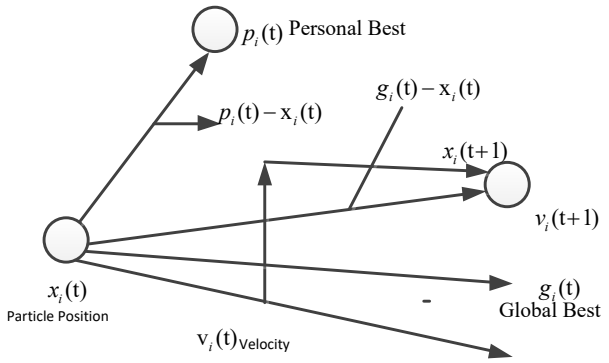

Figure 11 Searching mechanism of the PSO algorithm

The parameters of the proposed SMES and TCSC obtained by the PSO optimization Technique are given in Table 1. The internal structure of the PD-PID controller is demonstrated in Figure 10

Table 1 SMES and TCSC optimized Parameter obtained By PSO (PSO-PD-PID)

S.NO	Parameters of SMES	Case-01	Case-02	Case-03	Case-04
1	K_1	1.9958	1.9613	1.0952	1.8768
2	K_2	1.9990	1.9854	1.9012	1.7899
3	K_3	1.9958	1.9998	1.9031	1.29567
4	K_2	1.9999	1.9321	1.1588	1.9730
5	K_{SMES}	0.4004	0.3670	0.7191	0.6802
6	T_{SMES}	0.0432	0.0309	0.0630	0.0441

S.NO	Parameters of TCSC	Case-03	Case-04
1	K_{TCSC}	1.8652	1.7641
2	T_{TCSC}	0.0921	0.08712

Table 2 Comparison of all cases based on Performance indices Proposed (PSO-PD-PID)

S.NO	cases	ITAE	ITSE	IAE	ISE
1	LFC-AVR-SMES	2.2853	0.1957	1.5509	0.727
2	LFC-AVR-HVDC-SMES	1.9136	0.1892	1.4658	0.630
3	LFC-AVR-TCSC-SMES	1.7122	0.1762	1.3429	0.520
4	LFC-AVR-TCSC-HVDC-SMES	1.6843	0.1349	1.2468	0.424

Table 3 Results Obtained By Proposed PSO-PD-PID, Based On Settling-Time Cases Are Compared

S.NO	cases	Δf_1	Δf_2	ΔP_{12}	Δv_1	Δv_2
1	Case-01	14.4	13.543	19.953	3.9465	1.791
2	Case-02	8.26	8.2579	9.2479	1.4052	1.568
3	Case-03	7.37	7.6972	6.3351	1.3035	1.391
4	Case-04	7.52	5.0937	5.8351	1.1682	1.169

Table 4 Results Obtained By Proposed PSO-PD-PID, Based On Peak-Time Cases Are Compared

S.NO	cases	Δf_1	Δf_2	ΔP_{12}	Δv_1	Δv_2
1	Case-01	1.38	1.082	2.0632	2.084	2.304
2	Case-02	0.88	0.771	1.1688	1.628	1.957
3	Case-03	0.44	0.646	0.4425	0.490	1.316
4	Case-04	0.03	0.0075	0.00701	0.3014	0.6013

Table 5 Comparison of Proposed PSO-PD-PID) controller demonstrated for (LFC-AVR-HVDC-TCSC-SMES) (case-04)based on Settling-Time from Recent published literature

S.No	Parameters of system	Proposed PD-PID controller for (case-04)	DEPSO-PID[20]	HAEFA-PID[19]	QEQS-PID[25]	IWO-PID[26]	PSO-PID[24]
1	ΔF_1	7.0852	15.21	8.076	7.539	8.577	7.790
2	ΔF_2	5.0937	6.877	11.68	12.94	8.567	9.108
3	ΔP_{12}	5.8351	17.07	19.78	11.22	15.45	21.7
4	ΔV_1	1.1682	3.954	2.150	3.518	3.978	2.49
5	ΔV_2	1.1669	2.466	2.740	3.875	3.149	3.93

Table 6 Eigenvalues for all four proposed cases

s.no	Case-01	Case-02	Case-03	Case-04
1	-3.33 + 0.00i	-3.33 + 0.00i	-3.33 + 0.00i	-3.33 + 0.00i
2	-0.10 + 0.00i	-0.10 + 0.00i	-0.10 + 0.00i	-0.10 + 0.00i
3	-3.33 + 0.00i	-3.33 + 0.00i	-3.33 + 0.00i	-3.33 + 0.00i
4	-0.10 + 0.00i	-0.10 + 0.00i	-0.10 + 0.00i	-0.10 + 0.00i
5	-8.07 + 0.00i	-08.060 - 0.00i	-8.095 + 0.0i	-8.01 + 0.00i
6	-1.063 + 0.0i	-0.8020 + 0.0i	-8.074 + 0.0i	-8.071 + 0.00i
7	-1.96+ 0.0i	-2.206 + 0.0i	-2.09 + 0.0i	-20.51 + 0.0i
8	-1.96 + 0.00i	-1.984 + 0.00i	-1.86 + 0.00i	-2.69+ 9.340i
9	-1.9 + 0.0i	-1.44 + 0.0i	-1.3 + 0.0i	-2.10 + 9.340i
10	-1.93 + 0.0i	-1.30 + 0.0i	-1.97 - 0.0i	-19.031 +0.0i
11	-3.01 + 7.98i	-2.869 + 10.9i	-7.089+6.71i	-19.13 + 0.0i
12	-3.02 + 7.98i	-2.89 + 10.8i	-7.09 + 6.75i	-19.04 - 0.0i
13	-3.06 + 7.95i	-3.16 + 7.920i	0.99 + 7.66i	-3.79 + 7.10i
14	-3.03 +7.91i	-3.136 + 7.96i	0.95+ 7.616i	-3.749 + 7.10i
15	-12.84 + 0.0i	-12.4 + 0.0i	-13.64 + 0.0i	-12.49 + 0.00i
16	-12.81 + 0.0i	-12.74 + 0.0i	-12.80 + 0.0i	-12.2 + 0.0i
17	-1.26 + 0.00i	-12.41 + 0.00i	-13.69 + 0.0i	-12.50 + 0.00i
18	-1.250 - 0.0i	-12.5+ 0.0i	-12.50+ 0.0i	-12.84 + 0.0i
19	-5.32 + 1.32i	-3.740 + 4.20i	-12.49 + 0.0i	-7.064 + 0.00i
20	-5.02 + 1.31i	-3.10 + 4.21i	-12.14+ 0.0i	-3.065 - 7.90i
21	-5.301 + 0.0i	-6.8847 + 0.0i	-7.482 + 0.0i	-3.07 +7.909i
22	-0.20+ 3.331i	-4.972 + 1.23i	-0.10 + 3.74i	-0.08 + 3.396i
23	-0.60 + 3.32i	-4.902 + 1.23i	-0.17 + 3.72i	-0.408 +3.36i
24	-0.66 + 3.30i	-0.645 + 3.36i	-3.112 + 0.0i	-5.01 + 1.407i
25	-0.66 + 3.35i	-0.636 + 3.31i	-0.27 + 3.9i	-5.05 + 1.07i
26	-1.52 + 1.88i	-0.639+ 3.353i	-0.21+ 3.95i	-3.07 + 0.0i
27	-1.57 + 1.86i	-0.639 +3.383i	-0.12 + 3.6i-	-0.65 + 3.37i
28	-3.37 + 0.0i	-3.95 + 0.0i	-0.16 - 3.60i	-0.63 + 3.378i
29	-3.01 + 0.0i	-3.05569+ 0.0i	-3.155 + 0.0i	-3.05 + 0.0i
30	-2.36 + 0.0i	-1.103+ 0.0i	-2.01 + 0.0i	-1.13 + 0.116i
31	-0.81 + 0.42i	-1.07 - 0.3894i	-1.515 + 0.0i	-1.34- 0.16i
32	-0.80 + 0.42i	-0.81+ 0.5229i	-1.45 + 0.00i	-1.06+ 0.00i
33	-1.016 + 0.0i	-0.374+ 0.529i	-1.109 + 0.0i	-1.446 + 0.0i
34	-0.14 + 0.0i	-0.917+ 0.000i	-0.78 + 0.0i	-0.600 + 0.0i
35	-1.2 + 1.9i	-0.98+ 0.0i	-0.602 + 0.0i	-0.601 + 0.08i
36	-1.4 + 1.3i	-1.41+ 0.0i	-0.586 + 0.0i	-0.82 + 0.491i
37	-0.401 + 0.0i	-1.492 + 0.0i	-0.803 + 0.0i	-0.802 + 0.0i
38	-0.105 + 0.0i	-0.302 + 0.0i	-1.267 + 0.0i	-0.298 + 0.0i
39	-0.051 + 0.0i	-0.505 + 0.0i	-1.407 + 0.0i	-0.933 + 0.0i
40	-0.010 + 0.0i	-0.05 + 0.0i	-1.201 + 0.0i	-0.105 + 0.0i
41	-0.060 + 0.0i	-0.026 + 0.0i	-0.919 + 0.0i	-0.101+ 0.0i
42	-0.091+ 0.0i	-0.0610+ 0.0i	-0.701 + 0.0i	-0.010 + 0.0i
43	-0.02 + 0.0i	-0.091 + 0.0i	-0.24 + 0.0i	-0.02 + 8.3i
44	-0.02 + 0.01i	-0.014 + 0.0i	-0.018 + 0.0i	-0.091 + 8.38i
45	-0.01+ 0.003i	-0.052 + 0.03i	-0.097 + 0.0i	-0.0360 + 0.0i
46	-0.04 + 0.10i	-0.02 - 0.011i	-0.091 + 0.0i	-0.014 + 0.03i
47	-0.003 +0.03i	-0.001 + 0.03i	-0.03 + 0.0i	-0.012 + 0.01i
48	-1.33 + 0.00i	-0.052 + 0.32i	-0.01 + 0.01i	-0.02 + 0.010i
49	-1.805 + 0.0i	-1.90 + 0.000i	-0.05 - 0.06i	-0.052 +0.10i
50	-3.814 + 0.0i	-1.506 + 0.00i	-0.01 + 0.07i	-2.431 + 0.00i
51	-6.51 + 0.00i	-1.33 + 0.00i	-0.01 + 0.01i	-2.43 + 0.00i
52	-0.01 + 0.0i	-3.32 + 0.00i	-4.42 + 0.00i	-1.88+ 0.000i
53	-0.769 + 0.0i	0.0011 + 0.0i	-3.38 + 0.0i	-5.405 + 0.0i
54	-0.010 + 0.0i	-0.7669 + 0.0i	-0.769 + 0.0i	-0.0011 + 0.0i
55	-0.667 + 0.0i	-0.0010 + 0.0i	-0.667 + 0.0i	-0.7632 + 0.0i
56	-3.333 + 0.0i	-0.67 + 0.0i	-3.333 + 0.0i	-0.0016 + 0.0i
57	-0.10 + 0.0i	-3.333 + 0.0i	-0.100 + 0.0i	-0.665 - 0.06i

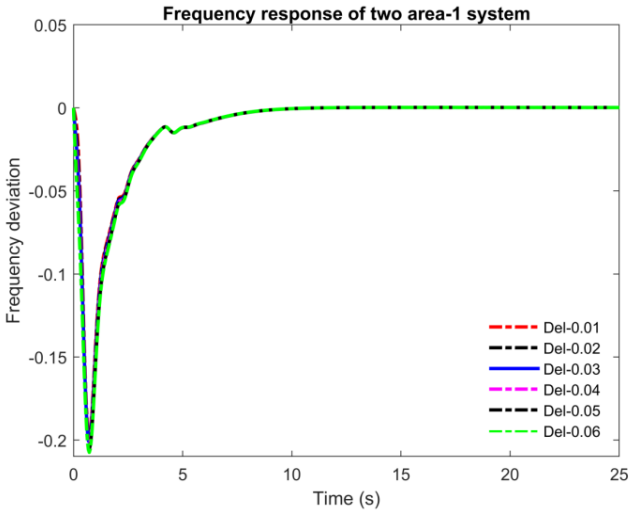

Figure 12 Frequency Variation at Different Step Load Perturbation (SLP) for area-1(case-04)

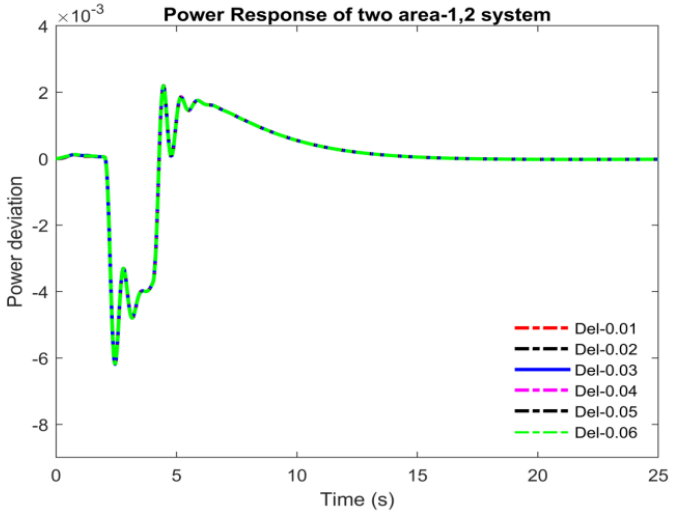

Figure 13 Power variation at Different Step Load Perturbation (SLP) For area-1,2 (case-04)

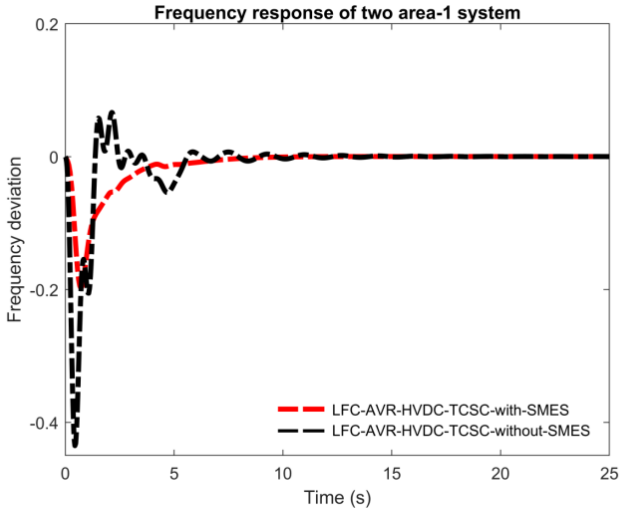

Figure 14 Frequency Deviation Response (area-1) with and without SMES for case-04

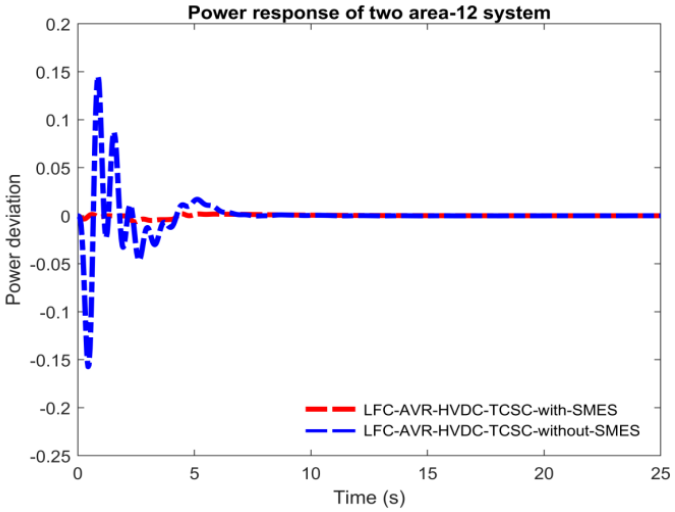

Figure 15 Power Deviation Response (area-1, 2) with and without SMES for case-04

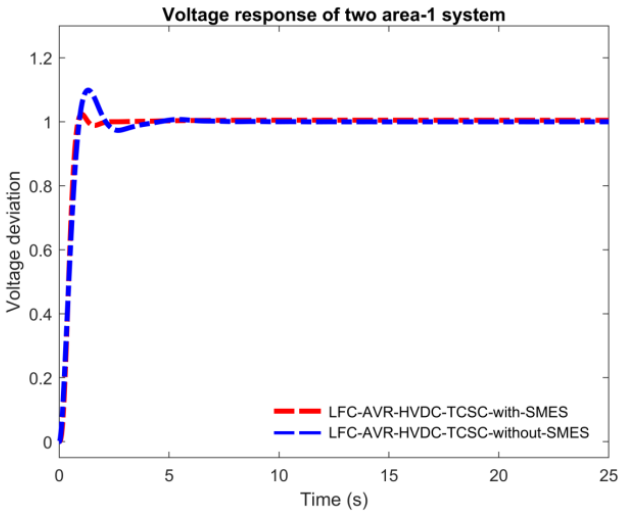

Figure 16 Voltage Deviation Response (area-1) with and without SMES for case-04

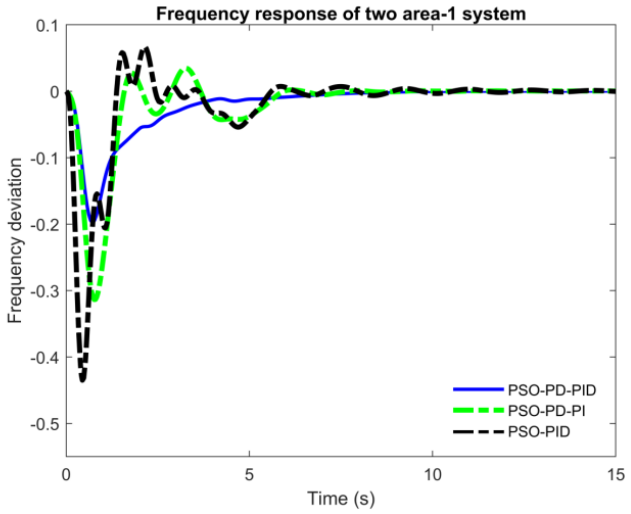

Figure 17 Frequency responses for area-1 obtained by different proposed controllers For Case-04

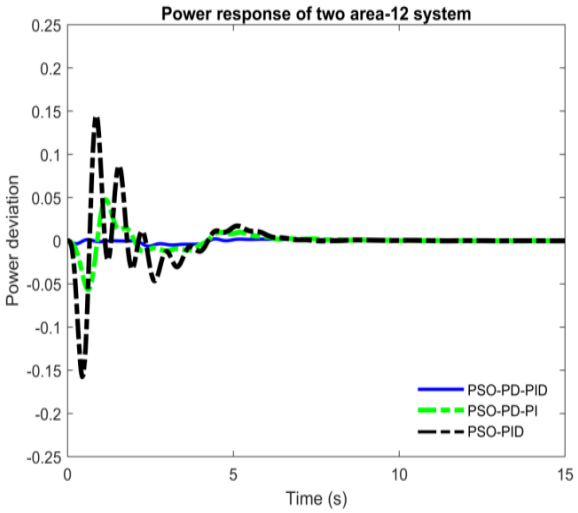

Figure 18 Power response for area-1,2 obtained by different Proposed controllers For Case-04

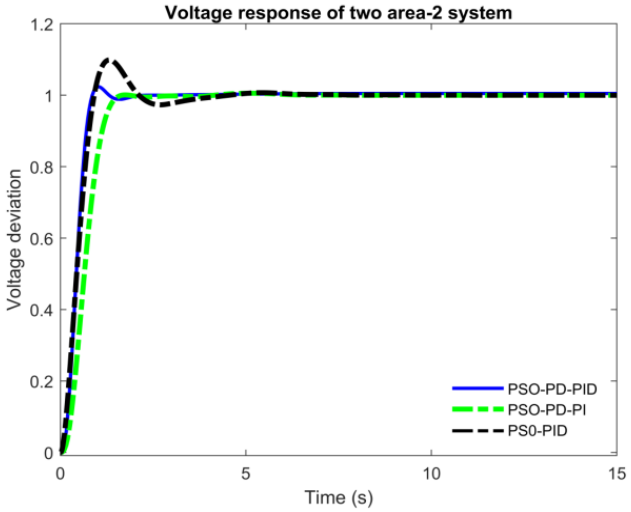

Figure 19 Voltage responses for area-2 obtained by different proposed controllers For Case-04

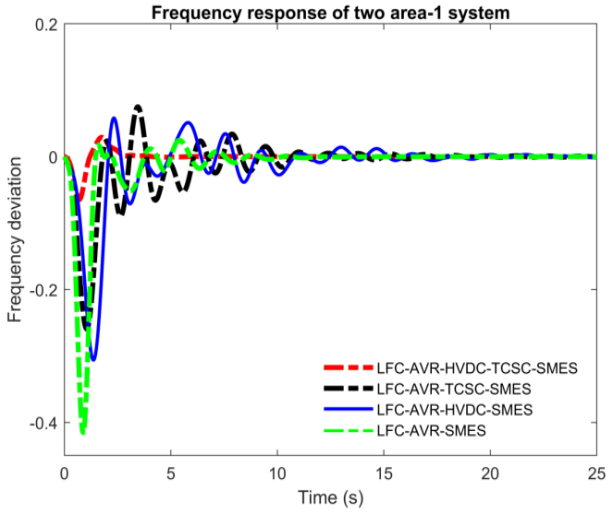

Figure 20 Frequency response for area-1 of different cases obtained by Proposed PSO-PD-PID controller

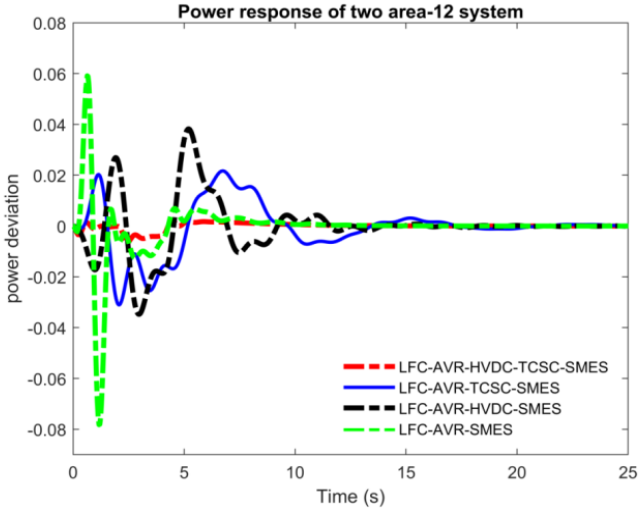

Figure 21 Power response for (area-1,2) of different cases obtained by Proposed PSO-PD-PID controller

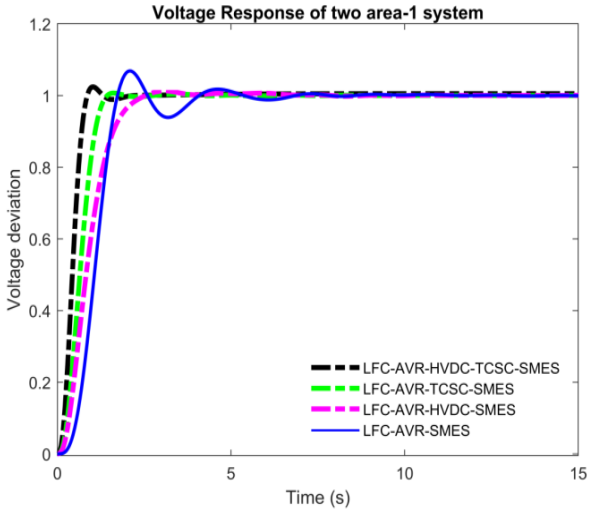

Figure 22 Voltage response for area-1 at different cases obtained by Proposed PSO-PD-PID controller

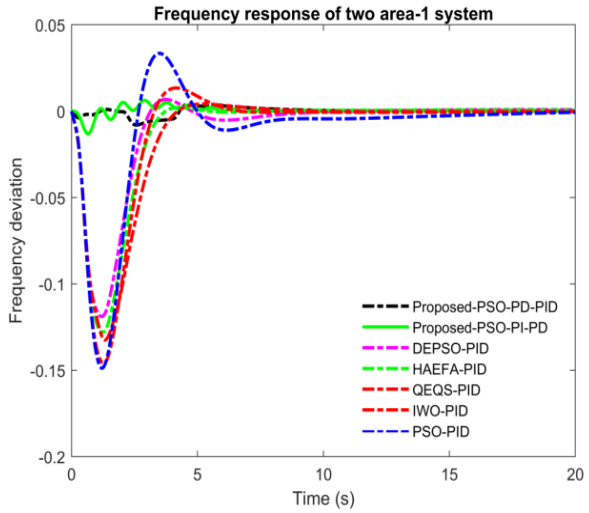

Figure 23 Frequency Response comparison of proposed controllers with Different Tuned PID controllers of Published literature for area-1 [19, 20, 24-26]

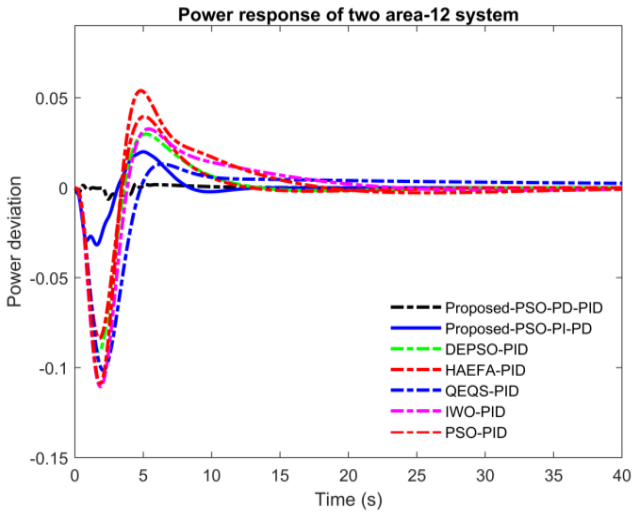

Figure 24 Power Response comparison of proposed controllers with Different Tuned PID controllers of Published literature for area-1,2 [19, 20, 24-26]

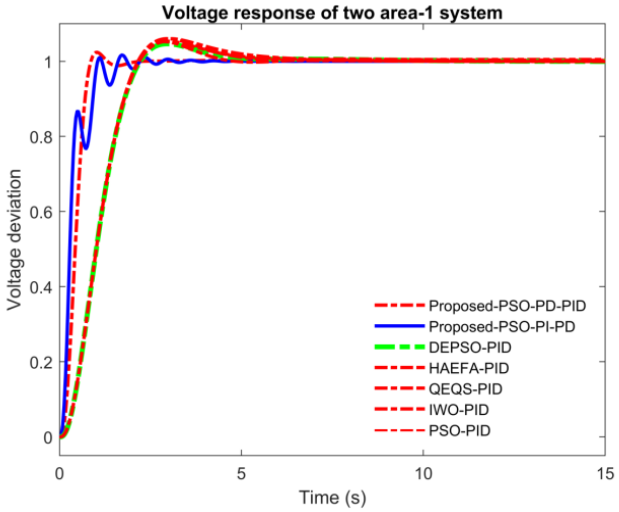

Figure 25 Voltage Response comparison of proposed controllers with Different Tuned PID controllers of Published literature for area-1[19, 20, 24-26]

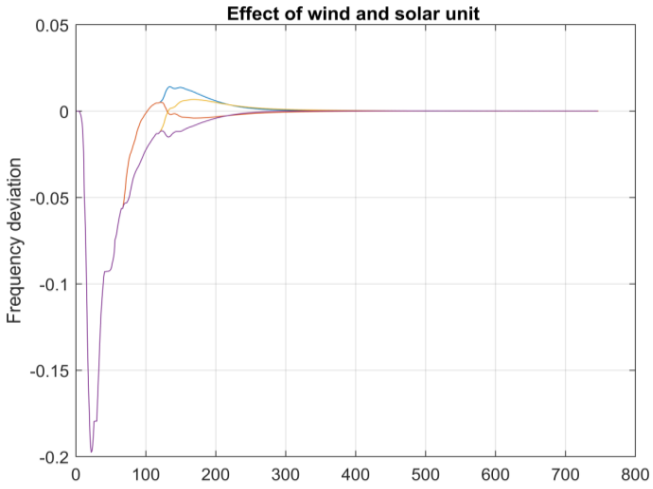

Figure 26 Effect of wind and solar units, Step input variation on Frequency response for area-1

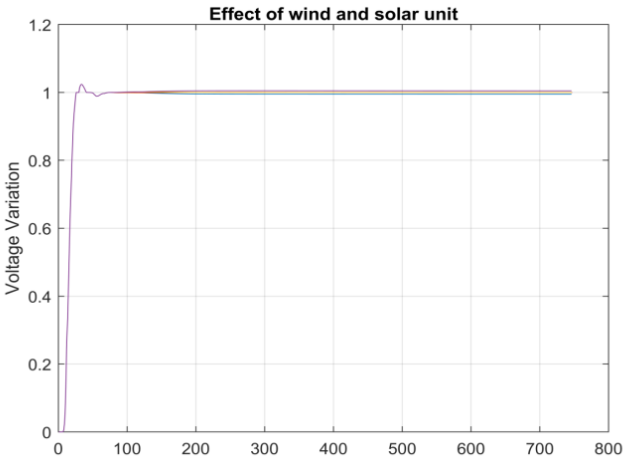

Figure 27 Effect of wind and solar units, Step input variation on Voltage response for area-1

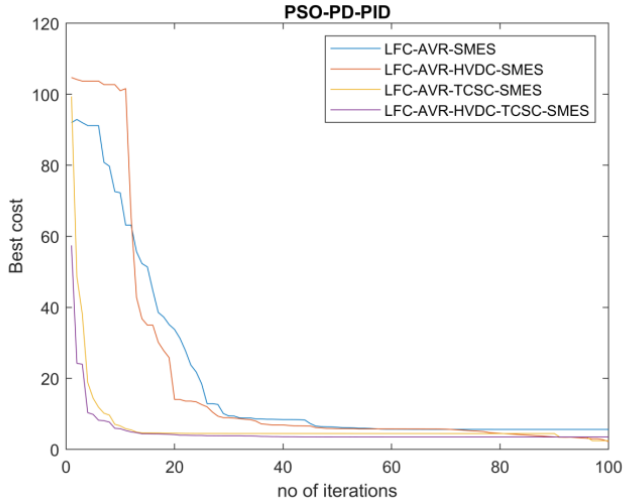

Figure 28 Iteration graph of different cases obtained while optimizing PD-PID controller Parameters

5.0 RESULT DISCUSSION

In this article, MAMS-IPS with renewable sources is considered for LFC. Solar and wind energy sources are incorporated with MAMS-IPS. This paper is divided into four different cases. In case-01 LFC-AVR-MAMS-IPS with SMES is considered for study. In the second case effect of the HVDC link with AC link is observed. In the third case effect of the Fact device (TCSC) is seen. In case-04 combined effect of HVDC and TCSC with SMES is considered. By applying facts device intergated with SMES deviation in output responses is mitigated upto a desirabe value near to zero.

The robustness of the proposed (PD-PID) controller is verified by varying the step load. Step load is increased by 10%, the effect of varying load can be seen in *Figure 12* and *Figure 13*. 0.01 p.u step load is given to each area. Frequency and power response do not change much as the load is varied. The steady-state error of the response remained almost zero.fluctuation in Tie-line power and frequency response is very less as load is varied. Controller rigidness is tested for all four cases, in this article case-04 result are portrayed.

The effect of SMES is shown in *Figure 14* and Figure 15. By absorbing the responses it is seen by incorporating the SMES with MAMS-IPS the deviation in the response is minimized. The settling time and peak time of the response are minimized to a great extent. *Figure 16* shows voltage response output with and without SMES for MAMS-IPS; the Peak Time (PT) of the response is reduced. Result investigated for case-04 are illustrated in this study showing effect of SMES. *Figure 17* to *Figure 19* the effect of proposed controllers is seen as in this study three controllers are taken into consideration. Conventional PID controller, PI-PD controller, and PD-PID controller parameters are optimized using nature-inspired algorithm (PSO). *Figure 18 illustrate resposes of different controller implemented for case-04*. PD-PID controller shows superiority over the other suggested controller. This controller's comparison is done for all different cases. In this arrticle result of case-04 is demostrated. The settling time and peak time of the response is decreased effectively as compared to the proposed PID/PI-PD controller.

In all four cases PD-PID controller is implemented and *Figure* 20 to *Figure* 22 shows the comparison of all four cases, in this output response obtained by applying proposed PD-PID controller is taken into consideration. *Figure 21 demonstrate the power respose of area 1,2 obtained by intelligent controller.* case-04 shows more effectiveness as compared to other cases used for the LFC study. The steady-state error is reduced and the Settling-Time (ST) and Peak-Time (PT) of the responses obtained by case-04 are minimized more as compared to the other proposed cases. So by this it is concluded that by implementing SMES-TCSC-HVDC in PS the performance of the electrical system is enhanced and deviation of output responses is minimized to a acceptable value.

A comparison of the proposed controller with the recently published optimal controller is absorbed in Figure 23 to Figure 25. Comparision of power response of case-04 with resectly published literature controller is shown by Figure 24. An optimized PD-PID controller shows superiority. Settling-Time and Peak overshoot is minimized in the output response. The system used in the literature For the LFC study is similar to the power system model of this article. The effect of wind unit and solar unit is seen in Figure 26 and Figure 27 as the value of step input given to solar and wind unit in the form of step load is varied by $\pm$ 10%. The response of frequency and voltage varies as input to the renewable source is varied. But steady-state error remains near zero by this rigidness of the proposed controller is also tested. Result obtained by suggested (PSO-PD-PID) controller is only shown in this presented work. Iteration graphs obtained while optimizing the (PSO-PD-PID) for all four cases are illustrated in Figure 28. The optimized gain of TCSC and SMES obtained by PSO optimized technique is given in Table 1. Table 2 shows the comparative results of all four cases based on performance indices. Case-04 shows better results as compared to other suggested cases. Based on ITAE, IAE, ITSE, and ISE the comparison is done. The result of the PSO-PD-PID controller is taken into consideration in this comparison. Based on Settling Time (ST) and peak overshoot time result of all four cases is compared and this comparison is demonstrated in *Table 3* and *Table 4*. When different cases illustrated in *Table* 3 are compared with each other it is concluded that setlling time of area-1 (Δf_1) responses is reduced by 47.7%, similarly (ST) of (Δf_2) is minimized by 62.38%. (ST) of power deviation response ($\Delta P_{1,2}$) is reduced by 70.5 % of case-04 when compared with case-01. (ST) of (ΔV_1) response is improved by 70.5 % of case-04 as compared with case-01. Settling Time of (ΔV_2) is decresed by 34.47 % of case-04 when compared with case-01. By this discussion it is observed that case-04 (LFC-AVR-SMES-HVDC-TCSC) improves the response output as compared with case-01. Peak overhoot of responses obtained by case-04 is comapred with case-1 is demomstraed in *Table 4*, percenatge decrement in peak overshoot (PO) is very promissing, (Δf_1) response percenatge decrement is 97.91%. similarly (Δf_2) peak overshoot (PO) is reduced by 93.06% obtained by case-04 when compared with case-01, ($\Delta P_{1,2}$) response (PO) is minimized by 98.83 %.(ΔV_1) response (PO) is reduced by 85.55% which is gained by case-04. (ΔV_2) response (PO) is decresed by 74.03 % of case-04.

Results obtained by implementing (PSO-PD-PID) controller for case-04 are compared with the recently published optimal controller and their comparison is shown in *Table 5* based on Settling Time. By this comparision it is concluded that output response of the PS is improved very effiently. For seeing the stability of the proposed power system models eigenvalue analysis is evaluated. Eigenvalues for all the cases are demonstrated in *Table 6*, By absorbing the Table it is analysed that all values are locatred in the left s-plane by this stability of the system is verified.

6.0 CONCLUSION

In this paper analysis of dynamic performance of the LFC is done. Four different cases are considered in this article. Generating units such as thermal, hydro, and gas followed by wind and solar unit is taken into consideration. Effect of implementing HVDC link with AC-Link and Fact Device (TCSC) on frequency and Tie-Line power is absorbed. An optimized PD-PID controller is incorporated with SMES to improve the dynamic output responses of the MAMS-IPS. A comparison of the optimized PD-PID controller with the optimal PID/PI-PD controller is done; it is found that PSO-PD-PID shows superiority over other suggested controllers. A comparison of the proposed controller with a recently published optimal controller is also conducted to see the effectiveness of the suggested controller for LFC. The effect of solar-unit and wind-unit is also absorbed by applying a step input of $\pm$ 10% to each unit and varying it. The robustness of the proposed controller is verified by applying different step loads in terms of per unit to each area. Objective functions ITAE, ISE, IAE, and ITSE are taken into consideration for optimizing the parameters of the proposed controllers. Parameters of TCSC and SMES are also optimized using nature-inspired algorithm optimization techniques. Effects of nonlinearity such as GDB, GRC, and Boiler are considered in each area. The effect of magnetic energy storage (SMES) devices on the output responses of LFC is also observed. Eigenvalue analysis is also taken into consideration to see the stability of the proposed Power system model. This study can be further enhanced by using different generating units such as nuclear,diesel and other renewable unit such as geothermal. A novel optimizing technique and cascade controller can be implemented for enhanching the study.

Appendix

$f = 50$ Hz; $B_1 = B_2 = B = 0.45$ MW/Hz;
$P_R = 2000$ MW(rating), $P_L = 1740$ MW(smallloading);
$R_1 = R_2 = R_3 = 2.4$ Hz/p.MW; $pf_{11} = pf_{21} = 0.49666$;
$pf_{12} = pf_{22} = 0.37814$; $pf_{13} = p_{23} = 0.1522$;
$T_{pu} = 11.49$; $K_{pu} = 68.9566$ Hz/p.u,
$T_{12} = 0.0433$; $a_{12} = -1$.

Thermal: $T_{gr} = T_{gr} = T_{gr} = 0.08$ sec;

$T_{re1} = T_{re2} = T_{re} = 10$ sec;

$K_{r1} = K_{r2} = K_r = 0.3$, $T_{tr} = T_{tr} = 0.3$ sec.

Hydro: $T_{h1} = T_{h2} = T_h = 28.75$,sec, $T_{rs1} = T_{rs2} = T_{rs} = 5$ sec; $T_{rh1} = T_{rh2} = T_{rh} = 0.2$ sec; $T_{w1} = T_{w2} = T_w = 1$ sec.

Gas: $b_1 = b_2 = b = 0.5$ sec; $c_1 = c_2 = c = 1$ sec;

$X_1 = X_2 = X = 0.6$ sec;

$Y_1 = Y_2 = Y = 1$ sec; $T_{cr1} = T_{cr2} = T_{cr} = 0.03$ sec;

$T_{f1} = T_{f2} = T_f = 0.23$ sec; $T_{cd1} = T_{cd2} = T_{cd} = 0.2$ sec

AVR models parameters .The time and gain constants of the amplifier are $K_A = 10, T_A = 0.1$ sec, the exciter time constant $K_E = 1, T_E = 0.4$ sec, the generator time constant $K_G = 0.8, T_G = 1.4$, gain and time constant of thesensor $K_s = 1, T_s = 0.05, P_s = 1.5$,

$K_1 = 0.2, K_2 = -0.2, K_3 = 0.5, K_4 = 1.4$

Renewable-units:

$K_{pv} = 1,\ T_{pv} = 1.5,\ K_{WT} = 1,\ T_{WT} = 1,$ HVDCunit:

$K_{dc} = 1,\ T_{dc} = 0.8,$

Acknowledgement

The researcher would like to thank the Electrical Engineering Department for providing the facilities required for this research, as well as the simulation software. Special thanks also go to Rajasthan Technical University (RTU), Kota, India, for providing the resources necessary to conduct this research work

References

[1] S. K. Pandey, S. R. Mohanty, and N. Kishor, 2013, "A literature survey on load–frequency control for conventional and distribution generation power systems," *Renewable and Sustainable Energy Reviews,Elsevier,* 25(4): 318-334, doi: 10.1016/j.rser.2013.04.02.

[2] A. Sree Vidya, V. Bharath Kumar, Y. V. Pavan Kumar, D. John Pradeep, and C. Pradeep Reddy, 2023, "Design of Automatic Load Frequency Control Loop Using Classical PID Control Methods," Springer Nature Singapore, in Control Applications in Modern Power Systems, 3(2): 153-176, doi: 10.1007/978-981-19-7788-6_11.

[3] S. Debbarma, L. C. Saikia, and N. Sinha, 2014, "Robust two-degree-of-freedom controller for automatic generation control of multi-area system," *International Journal of Electrical Power & Energy Systems,* 63(4): 878-886, doi: 10.1016/j.ijepes.2014.06.053.

[4] E. Çelik, N. Ozturk, Y. Arya, and C. Ocak, 2021, "(1 + PD)-PID cascade controller design for performance betterment of load frequency control in diverse electric power systems," *Neural Computing and Applications,* 33(4): 1-12, doi: 10.1007/s00521-021-06168-3.

[5] N. K. Gupta, M. K. Kar, and A. K. Singh, 2022, "Design of a 2-DOF-PID controller using an improved sine–cosine algorithm for load frequency control of a three-area system with nonlinearities," *Protection and Control of Modern Power Systems,* 7(1): 23-33, doi: 10.1186/s41601-022-00255-w.

[6] P. N. Topno and S. Chanana, 2018, "Load frequency control of a two-area multi-source power system using a tilt integral derivative controller," *Journal of Vibration and Control,* 24(1): 110–125, doi: 10.1177/1077546316634562.

[7] D. Tripathy, A. K. Barik, N. B. D. Choudhury, and B. K. Sahu, 2019, "Performance Comparison of SMO-Based Fuzzy PID Controller for Load Frequency Control," Singapore,Springer Singapore, in *Soft Computing for Problem Solving,* 14(4): 879-892, doi: 10.1007/978-981-13-1595-4_70.

[8] D. Sambariya and V. Nath,2016. "Load frequency control using fuzzy logic based controller for multi-area power system," *British Journal of Mathematics & Computer Science,*13(5): 1-19, doi: 10.9734/BJMCS/2016/22899.

[9] V. Nath and D. Sambariya, 2015, "Analysis of AGC and AVR for single area and double area power system using fuzzy logic control," International Journal of Advanced Research in *Electrical, Electronics and Instrumentation Engineering,* 7(4): 6501-6511, doi: 10.15662/ijareeie.2015.0407075.

[10] V. Nath and D. K. Sambariya, 2016, "Design and performance analysis of adaptive neuro fuzzy controller for load frequency control of multi-power system," *International Conference on Intelligent Systems and Control* (ISCO), 16(4): 1-7, doi: 10.1109/ISCO.2016.7726986.

[11] D. K. Sambariya and V. Nath, 2016, "Application of NARMA L2 controller for load frequency control of multi-area power system," *International Conference on Intelligent Systems and Control (ISCO),* 16 (4): 1-7, doi: 10.1109/ISCO.2016.7726987.

[12] D. Sambariya and V. Nath, 2015, "Optimal control of automatic generation with automatic voltage regulator using particle swarm optimization," *Universal Journal of Control and Automation,* 3(4): 63-71 , doi: 10.13189/ujca.2015.030401

[13] P. Bhatt, R. Roy, and S. Ghoshal, 2011, "Comparative performance evaluation of SMES–SMES, TCPS–SMES and SSSC–SMES controllers in automatic generation control for a two-area hydro–hydro system," I*nternational Journal of Electrical Power & Energy Systems,* 33(10): 1585-1597, doi: 10.1016/j.ijepes.2010.12.015.

[14] D. K. Lal and A. K. Barisal, 2017, "Comparative performances evaluation of FACTS devices on AGC with diverse sources of energy generation and SMES," *Cogent Engineering,* 4 (1): 131-139, doi: 10.1080/23311916.2017.1318466.

[15] M. Sharma, S. Prakash, and S. Saxena, 2021,"Robust Load Frequency Control Using Fractional order TID-PD Approach Via Salp Swarm Algorithm," *IETE Journal of Research,* 69(5): 2710-2726 , doi: 10.1080/03772063.2021.1905084.

[16] R. K. Sahu, T. S. Gorripotu, and S. Panda, 2015, "A hybrid DE–PS algorithm for load frequency control under deregulated power system with UPFC and RFB," *Ain Shams Engineering Journal*, 6(3): 893-911, doi: 10.1016/j.asej.2015.03.011.

[17] R. Shankar, R. Bhushan, and K. Chatterjee, 2016, "Small-signal stability analysis for two-area interconnected power system with load frequency controller in coordination with FACTS and energy storage device," *Ain Shams Engineering Journal,*7(2): 603-612, doi: 10.1016/j.asej.2015.06.009.

[18] P. C. Pradhan, R. K. Sahu, and S. Panda, 2015, "Firefly algorithm optimized fuzzy PID controller for AGC of multi-area multi-source power systems with UPFC and SMES," *Engineering Science and Technology, an International Journal,*19(1): 338-354, doi: 10.1016/j.jestch.2015.08.007.

[19] C. Kalyan and G. S. Rao, 2020, "Coordinated SMES and TCSC Damping Controller for Load Frequency Control of Multi Area Power System with Diverse Sources," *International Journal on Electrical Engineering&Informatics,* 12(4): 1-14 doi: 15676/ijeei.2020.12.4.4.

[20] D. K. Lal, A. K. Barisal, and M. Tripathy, "Load frequency control of Multi Source Multi-Area nonlinear power system with DE-PSO Optimized Fuzzy pid controller in coordination With SSSC and

RFB," *International journal Control and Automation*, 11(7): 61-80, doi: 10.14257/ijca.2018.11.7.06.

[21] R. K. Khadanga and A. Kumar, 2019 "Analysis of PID controller for the load frequency control of static synchronous series compensator and capacitive energy storage source-based multi-area multi-source interconnected power system with HVDC link," *International Journal of Bio-Inspired Computation,* 13(2): 131-139, doi: 10.1504/IJBIC.2019.098413.

[22] G. Paliwal, K. Parkh, and R. Jangid, 2020, "Load Frequency Control of Multi-Area Multi Source Power System by Gray Wolf Optimization Technique," *International Journal of Research in Engineering, Science and Management* 12(4): 1-12, 10.1016/j.asoc.2023.110135.

[23] N. S. Kalyan and G. Sambasiva Rao, 2020, "Frequency and voltage stabilisation in combined load frequency control and automatic voltage regulation of multiarea system with hybrid generation utilities by AC/DC links," *International Journal of sustainable energy,* (39)10: 1009-1029, doi: 10.1080/14786451.1797740.

[24] C. N. S. Kalyan, B. srikanth, and C.H Reddy, 2022, "Comparative performance assessment of different energy storage devices in combined LFC and AVR analysis of multi-area power system," *Energies,* 15(2): 629-645, doi: 10.3390/en15020629.

[25] Vigya, C. K. Shiva, B. Vedik, and V. Mukherjee, 2023, "Comparative analysis of PID and fractional order PID controllers in automatic generation control process with coordinated control of TCSC," *Energy Systems,* 14(1): 133-170, doi: 10.1007/s12667-021-00457-5.

[26] S. Mishra, A. K. Barisal, and B. C. Babu, 2019, "Invasive weed optimization-based automatic generation control for multi-area power systems," International Journal of Modelling and Simulation,39(3):190-202,doi:10.1080/02286203.2018.1554403.

[27] M. A. R. Shafei, A. N. Abd Alzaher, and D. K. Ibrahim, 2020, "Enhancing load frequency control of multi-area multi-sources power system with renewable units and including nonlinearities," Indonesian Journal of Electrical Engineering and ComputerScience,19(1):108-118,doi:10.11591/ijeecs.v19.i1.

[28] D. Guha, P. K. Roy, and S. Banerjee, 2018, "Application of backtracking search algorithm in load frequency control of multi-area interconnected power system," *Ain Shams Engineering Journal,* 9(2): 257-276, doi: 10.1016/j.asej.2016.01.004.

[29] A. Daraz, S. A. Malik, H. Mokhlis, I. U. Haq, G. F. Laghari, and N. N. Mansor, 2020, "Fitness dependent optimizer-based automatic generation control of multi-source interconnected power system with non-linearities," *IEEE ACCESS*, 8(3): 100989-101003, 2020, doi: 10.1109/ACCESS.2020.2998127.

[30] S. Tripathy, R. Balasubramanian, and P. Nair, 1992, "Effect of superconducting magnetic energy storage on automatic generation control considering governor deadband and boiler dynamics," *IEEE Transactions on Power systems,* 7(3): 1266-1273, doi: 10.1109/59.207343.

[31] A. Pappachen and A. P. Fathima, 2019, "Impact of SMES–TCSC Combination in a Multi-Area Deregulated Power System with GA-Based PI Controller," Journal of Control, Automation and Electrical Systems, 14(3): 1-13, doi: 10.1007/s40313-019-00492-9.

[32] M. Nandia, C. K. Shivab, and V. Mukherjeeb, 2017, "Frequency stabilization of multi-area multi-source interconnected power system using TCSC and SMES mechanism," Journal of Energy Storage, 6(2): 1-15 , doi: 10.1016/j.est.2017.10.018.

[33] Srinivasarathnam, C. Yammani, and S. Maheswarapu, 2019, "Load Frequency Control of Multi-microgrid System considering Renewable Energy Sources Using Grey Wolf Optimization," Smart-Science, 12(2): 1-21, doi: 10.1080/23080477.2019.1630057.

[34] S. A. M. Abdelwahab, M. Mohamed, M. Ebeed, and W. S. Abdellatif, 2022, "Equilibrium Optimizer and FLC of Two Area Load Frequency control with Multi-Source Generators System," International Journal of Renewable Energy Research (IJRER), (12)4: 2180-2188, doi: 10.1080/15567036.1898496.

[35] R.S. Ponnurangam, and Rajapandiyan, 2021, "Impact of demand management with load frequency control in distribution network with high penetration of renewable energy source," International Transaction on Electrical Energy System, 12(3): 1-31, doi: 10.1002/2050-7038.13066.

[36] M. K. Debnath, T. Jena, and R. K. Mallick, 2016 "Novel PD-PID cascaded controller for automatic generation control of a multi-area interconnected power system optimized by grey wolf optimization (GWO)," IEEE 1st International Conference on Power Electronics, Intelligent Control and Energy Systems (ICPEICES) 6(3): 1-6, doi: 10.1109/ICPEICES.2016.7853271.

[37] P. Satapathy, M. K. Debnath, and P. K. Mohanty, 2018, "Design of PD-PID Controller with Double Derivative Filter for Frequency Regulation," IEEE International Conference on Power Electronics, Intelligent Control and Energy Systems (ICPEICES) 6(2): 1142-1147, doi: 10.1109/ICPEICES.2018.8897276.

[38] B. Dhanasekaran, J. Kaliannan, A. Baskaran, N. Dey, and J. M. R. Tavares, 2023, "Load Frequency Control Assessment of a PSO-PID Controller for a Standalone Multi-Source Power System," *Technologies,* 11(1): 1-22, doi: 10.3390/technologies11010022.

[39] V. Dhawane and D. Bichkar, 2020, "Load frequency control optimization using PSO based integral controller," International Journal of Recent Technology and Engineering (IJRTE), 8(6): 97-103, doi: 10.35940/ijrte.E6749.038620.

[40] A. M. A. Soliman, M. Bahaa, and M. A. Mehanna, 2023, "PSO tuned interval type-2 fuzzy logic for load frequency control of two-area multi-source interconnected power system," Scientific Reports, 13(3): 1-15, doi: 10.1038/s41598-023-35454-4.